Parameter-Tuning-Free Two-Step Identification of Mechanical Parameters for PMSM Drives

Chengbo Yang, *Member, IEEE*, Wei Liu, *Senior Member, IEEE*, Songyan Niu, Jiahua Lyu, and Kwok Tong Chau, *Fellow, IEEE*

***Abstract*—Accurate identification of mechanical parameters holds great significance for optimizing control performance and monitoring working status in permanent magnet synchronous motor (PMSM) drives. This work proposes a parameter-tuning-free two-step mechanical parameter identification method using signal injection and algebraic operations. It is devised based on a non-lumped mechanical motion model that incorporates nonlinear and asymmetric friction modeling, which can accurately characterize real-world dynamics. More importantly, the proposed method circumvents the need for parameter adjustments, such as observer gain design and pole placement. With a two-step collaborative mechanism, the developed method is successfully implemented. In the first step, the open-loop speed response triggered by signal injection is exploited to accurately identify nonlinear friction along with the initial inertia value. With aiding from the results of the first step, the second step develops an online algebraic estimator to track the potentially time-varying load torque and inertia. Real-time experiments are conducted on a 1.2-kW practical PMSM drive system to validate the feasibility of the presented method.**

***Index Terms*—Mechanical parameters, identification, open-loop speed response, signal injection, algebraic estimator, permanent magnet synchronous motor (PMSM).**

I. INTRODUCTION

PERMANENT magnet synchronous motors (PMSMs) are garnering increasing attention due to their superior power density, large torque-to-inertia ratio, and high efficiency [1]-[3]. On account of these exceptional characteristics, PMSM-based drive systems have attained substantial deployment in numerous industrial applications, such as numerical control machine tools, electric vehicles, industrial robots, unmanned aircraft, and medical instruments. Mechanical parameters, including moment of inertia, load torque, and Coulomb and viscous friction coefficients, are typically unknown but serve a vital role in achieving high-reliability and high-dynamic PMSM drives [4], [5]. A growing variety of advanced control methods, such as speed-loop controller tuning [6]-[8], instantaneous acceleration/speed estimation [9], friction feedforward compensation [10], and lubrication/wear evaluation [11], are highly dependent on accurate knowledge of these mechanical parameters. Consequently, mechanical parameter identification (MPI) has attracted extensive research interests in both industry and academia.

Currently, numerous methods have been proposed to seek the precise determination of mechanical parameters. Existing MPI techniques can broadly be categorized into six groups: observer-based methods [12]-[14], extended Kalman filters (EKFs) [15], [16], recursive least squares (RLS) [17], [18], model reference adaptive systems (MRASs) [8], intelligent optimization algorithm (IOA)-based methods [19], [20], and time-domain response (TDR)-based methods [6], [21], [22]. These promising approaches not only offer a wealth of options for identifying mechanical parameters but also have yielded positive MPI results in PMSM drives. Nevertheless, despite continuous advancements in MPI techniques, currently available methods are still grappling with the following critical challenges:

Challenge I: Heavy burden of parameter adjustments

On the one hand, existing MPI methods generally require repeated trial-and-error adjustments to their own parameters to achieve identification convergence and superior estimation accuracy, as well as to guarantee stability. For instance, in observer-based methods, the sliding-mode observer-based MPI demands careful selection of switching and feedback gains [12], while the extended state observer-based MPI requires appropriate pole placement [3]. Similarly, the covariance matrix of EKF and RLS, as well as the adaptive gain of MRAS, exerts a significant influence on the stability and convergence of MPI, thus requiring meticulous design and tuning [8], [15], [17]. Existing TDR-based and IOA-based MPI methods are also unable to circumvent parameter adjustments. For example, in [21], the appropriate frequency and amplitude of the sinusoidal reference speed are supposed to be selected based on the specific characteristics of the PMSM drive system, guaranteeing the speed feedback contains sufficient inertia information. These parameter adjustments not only impose a heavy workload but also render the identification result subject to considerable uncertainty.

On the other hand, implementing existing MPI methods typically relies on a functioning closed-loop speed controller, which undoubtedly results in a workload of adjusting controller parameters. Tuning the speed controller generally requires identifying mechanical parameters (particularly the inertia) [6], [7], and yet a well-tuned speed controller serves as an indispensable prerequisite for achieving the identification of these parameters, posing a paradoxical situation. To address this dilemma, some MPI methods (e.g., [12]) pre-tune the speed controller through trial-and-error processes. However, the trial-and-error tuning is blind, time-consuming, and potentially unsafe. Additionally, several MPI methods (such as [6] and [21]) obtain approximate inertia by neglecting friction torques, thereby allowing for a rough pre-tuning of the speed controller before the identification. Unfortunately, the inertia acquired in this manner may exhibit a significant deviation (especially in the case of larger friction coefficients), rendering the speed controller dysfunctional. Recently, an advanced speed-controller-independent MPI method has been reported in [22], but this method needs careful selection of internal parameters, such as slopes of two incremental injection currents. Moreover, it only considers the constant-inertia and no-load operating condition.

Challenge II: Lack of a non-lumped identification model accounting for nonlinear and asymmetric friction modeling

Existing MPI methods tend to simplify the mechanical motion model by reducing the number of to-be-estimated parameters. These simplifications include, but are not limited to: *i*) adopting lumped modeling (for instance, treating friction torque and load

This work was supported in part by the Innovation and Technology Commission, Hong Kong SAR, China, under Grant ITP/025/24AP, and in part by The Hong Kong Polytechnic University under Grant P0048560. *(Corresponding author: Kwok Tong Chau.)*

The authors are with the Research Centre for Electric Vehicles and Department of Electrical and Electronic Engineering, The Hong Kong Polytechnic University, Hung Hom, Kowloon, Hong Kong, China (e-mail: chengbo.yang@polyu.edu.hk; wei.liu@polyu.edu.hk; songyan-nic.niu@polyu.edu.hk; jia-hua.lyu@polyu.edu.hk; k.t.chau@polyu.edu.hk).

torque as a single parameter in [7], and combining viscous friction torque and Coulomb friction torque into one parameter in [8] and [14]); *ii*) neglecting the friction asymmetry between forward and reverse rotations [6], [21]; *iii*) disregarding the nonlinear characteristics of friction [12], [13]. Although such simplifications make the model easier to handle and identify, they lead to a failure in capturing important information that can characterize the key features and physical states of the drive system. For instance, under the lumped modeling of load and friction torques, it becomes infeasible to separately extract precise information regarding external actual load torque and friction coefficients, resulting in failure to perceive the external contact torque and the true lubrication/wear state [10]. Furthermore, given that lumped parameter modeling is inherently challenged to precisely capture nonlinear dynamic characteristics [3], and other simplifications ignore real physical properties, significant parameter estimation errors may also occur during the actual implementation.

As a means of confronting this challenge, an MPI method proposed in [4] makes a positive contribution. It is devised based on a non-lumped mechanical motion model that can distinguish the load torque, Coulomb friction torque, and viscous friction torque, achieving enhanced accuracy. However, the identification model of this method neglects friction nonlinearity, which makes it challenging to accurately capture the actual friction, particularly under low-speed operating conditions. Besides, ignoring friction asymmetry also hinders further improvement in its accuracy [10]. To sum up, investigating a non-lumped identification model considering friction nonlinearity and asymmetry is of substantial significance for identifying precise mechanical parameters.

In this paper, a parameter-tuning-free two-step MPI method using signal injection and algebraic operations is proposed to cope with the above-stated **Challenges I** and **II**. Overall, the **main contributions** of this work include the following aspects.

1) Different from the currently available MPI methods, the proposed approach is free from parameter adjustment, thereby eliminating the time-consuming trial-and-error tuning process and significantly streamlining the implementation procedure. On the one hand, the presented method itself does not involve any to-be-adjusted parameters and relies solely on signal injection and algebraic operations to achieve the identification of mechanical parameters. On the other hand, the entire identification process successfully precludes the need for tuning the parameters of the speed controller.
2) Unlike existing MPI methods, a non-lumped mechanical motion model accounting for friction nonlinearity and asymmetry, which can distinguish the Coulomb friction coefficient, viscous friction coefficient varying with speed, inertia, and load torque, is developed to serve as the identification model, laying the foundation for the more precise and complete capture of mechanical parameters. The proposed method is designed based on the analytical expressions and time-integration formulas of this identification model, enabling the direct computation of mechanical parameters without resorting to asymptotic convergence arguments and Lyapunov stability theory.
3) A two-step collaborative mechanism is devised to identify the mechanical parameters. In the first step (Step I), open-loop speed responses, triggered by constant and zero *q*-axis current injections, are exploited to measure the Coulomb friction coefficient, viscous friction coefficient varying with speed, and initial inertia. In the second step (Step II), leveraging the identification result obtained from Step I, an online algebraic estimator, designed based on differential algebra theory (see [23] and therein), is proposed to achieve rapid and precise real-time tracking of the load torque and inertia, which may vary over time during the work operation of the PMSM system.

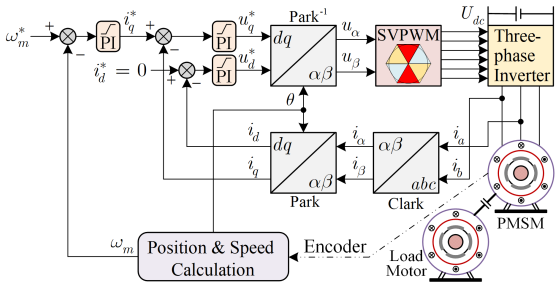

Fig. 1. Block diagram of the PMSM drive system under the FOC with $i_d^* = 0$.

The remaining sections of this paper are arranged as follows. Section II models the PMSM mathematically. Subsequently, Section III proposes the parameter-tuning-free two-step MPI method, accompanied by detailed theoretical analyses and derivations. Then, experimental investigations pertaining to the presented method are carried out in Section IV. Lastly, this paper is concluded in Section V.

II. Mathematical Modeling of PMSM

In the *dq*-axis reference frame, the mathematical model of a PMSM can be formulated as follows [4], [8], [21]:

$$u_q = R_m i_q + L_d p_n i_d \omega_m + L_q \dot{i}_q + \psi_m p_n \omega_m \tag{1}$$

$$u_d = R_m i_d - L_q p_n i_q \omega_m + L_d \dot{i}_d \tag{2}$$

$$J\dot{\omega}_m = T_e - T_L - B\omega_m - C\text{sign}(\omega_m) \tag{3}$$

where $i_d, i_q, T_e, u_d, u_q, p_n, R_m, \omega_m, L_d, L_q, \psi_m, B, J, C,$ and T_L denote the *dq*-axis currents, electromagnetic torque, *dq*-axis voltages, number of pole pairs, stator resistance, rotor speed, *dq*-axis inductances, magnet flux linkage, viscous friction coefficient, inertia, Coulomb friction coefficient, and load torque, respectively. Generally, in the real-world PMSM-driven system, the field-oriented control (FOC) with $i_d^* = 0$ is a widely-adopted control scheme. As illustrated in Fig. 1, this control scheme employs a dual-loop structure composed of a current loop and a speed loop. In this paper, we will focus on exploring the identification of mechanical parameters under the framework of FOC.

In practical applications, it is noteworthy that the viscous friction coefficient B exhibits variation with the motor speed and can be treated as a constant during high-speed motor operation [4], [24], [25]. Hence, B can be further expressed in detail as follows:

$$B = \begin{cases} f_B(\omega_m), & 0 \le |\omega_m| < a \text{(low-speed region)} \\ B_h, & a \le |\omega_m| \le \omega_{m\_\max} \text{(high-speed region)} \end{cases} \tag{4}$$

where B_h is a constant and stands for the viscous friction coefficient in the high-speed region; $f_B(\omega_m)$ is an unknown function pertaining to the rotor speed ω_m; $\omega_{m\_\max}$ is the maximum speed allowed by the real-world application (the allowable maximum speed of an actual application is typically constrained to its drive motor's rated speed, so as to ensure operational safety and reliability); a is a positive real number satisfying $a < \omega_{m\_\max}$, and it is essentially a boundary point for defining different friction characteristic regions in the actual PMSM drive system.

Furthermore, when accounting for the inconsistent viscous friction coefficient between the forward and reverse motor rotation due to the friction asymmetry [26], we can rewrite (4) as

$$B = \begin{cases} B^+ = \begin{cases} f_B^+(\omega_m), & 0 \le \omega_m < a^+ \\ B_h^+, & a^+ \le \omega_m \le \omega_{m\_\max} \end{cases} \\ B^- = \begin{cases} f_B^-(\omega_m), & -\omega_{m\_\max} \le \omega_m < -a^- \\ B_h^-, & -a^- \le \omega_m < 0 \end{cases} \end{cases} \tag{5}$$

where parameters with superscripts "+" and "−" correspond to

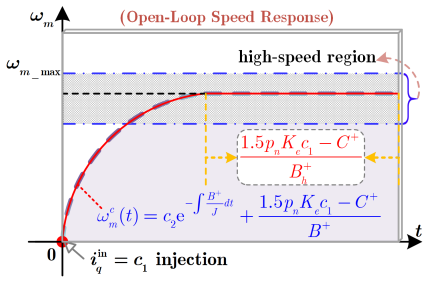

Fig. 2. Open-loop speed response that eventually stabilizes in the high-speed region under constant q-axis current injection.

the motor's forward and reverse rotation, respectively (e.g., B^+ refers to the viscous friction coefficient under the forward rotation). Similarly, C^+ and C^- are used to represent the Coulomb friction coefficient under the forward and reverse motor rotation, respectively. Hence, the PMSM system's mechanical motion model can be reformulated as

$$J\dot{\omega}_m = T_e - T_L - B^+\omega_m - C^+,\ (\omega_m > 0) \tag{6}$$

$$J\dot{\omega}_m = T_e - T_L - B^-\omega_m + C^-,\ (\omega_m < 0). \tag{7}$$

III. Proposed Identification Method

This section will develop a parameter-tuning-free two-step MPI method and elaborate its two-step identification process. Several appealing topics, such as open-loop speed response characteristic analysis, open-loop friction identification, speed-decay-based inertia estimation, online algebraic estimator design, and collaborative identification, will be covered.

A. Identification of Step I (Speed Loop Opened)

1) Open-Loop Identification of the Coulomb Friction Coefficient: In order to identify the Coulomb friction coefficient, this paper injects a constant current signal into the q-axis under the condition that the speed loop remains open, thereby utilizing the resulting open-loop speed response to determine C. This process involves neither adjustments to the algorithm's own parameters nor to the speed controller's parameters. Our proposed Coulomb friction coefficient identification algorithm is detailed below.

Generally, before the PMSM system is put into work operation, it can be reasonably thought that the load torque is zero and the inertia is constant [3], [10], [13]. Therefore, (6) and (7) can be simplified to

$$J\dot{\omega}_m = T_e - B^+\omega_m - C^+,\ (\omega_m > 0) \tag{8}$$

$$J\dot{\omega}_m = T_e - B^-\omega_m + C^-,\ (\omega_m < 0). \tag{9}$$

Next, this paper takes (8) as an example for further analysis. First, based on (8), we have the following result.

Theorem 1: If the q-axis injection current signal , i_q^{in} , is configured as $i_q^{\text{in}} = c_1$ (c_1 is a constant satisfying $c_1 > 0$), the resulting open-loop speed response will approach

$$\omega_m^c(t) = (1.5p_nK_ec_1 - C^+)\big/B^+ \tag{10}$$

where $\omega_m^c(t)$ is the open-loop speed response induced by injecting the constant q-axis current $i_q^{\text{in}} = c_1$; $K_e = [\psi_m - i_d(L_d - L_q)]$.

Proof: When the constant current $i_q^{\text{in}} = c_1$ is injected into the q-axis under the open-loop condition of the speed loop, we can calculate the electromagnetic torque T_e as $T_e = 1.5p_nK_ec_1$ [8]. Thereupon, (8) can be rewritten as

$$\dot{\omega}_m^c + (B^+\big/J)\omega_m^c = (1.5p_nK_ec_1 - C^+)\big/J. \tag{11}$$

Then, the analytical expression of (11) can be derived as

$$\begin{aligned}\omega_m^c(t) &= \mathrm{e}^{-\int (B^+/J)dt}\left\{c_2 + \int\left[(1.5p_nK_ec_1 - C^+)\big/J\right]\mathrm{e}^{\int (B^+/J)dt}dt\right\} \\ &= c_2\mathrm{e}^{-\int (B^+/J)dt} + (1.5p_nK_ec_1 - C^+)\big/B^+\end{aligned} \tag{12}$$

where c_2 is a constant, which depends on the initial value $\omega_m^c(0)$.

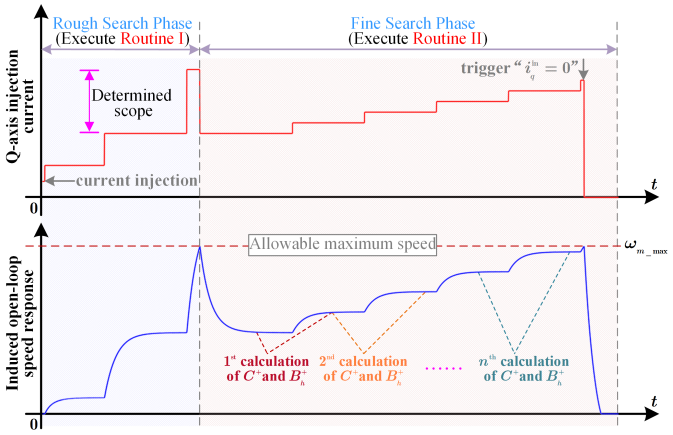

Fig. 3. Principle of the automatic search procedure for determining appropriate constant injection currents.

It can be noticed that the first term on the right-hand side of (12), which represents the transient speed response, will gradually tend to zero with increasing time. As this term diminishes, the final steady open-loop speed response can be derived as follows:

$$\omega_m^c(t) = (1.5p_nK_ec_1 - C^+)\big/B^+. \tag{13}$$

This ends the proof.

According to (13), it becomes apparent that when the injected constant q-axis current signal induces the final steady open-loop speed response to enter the high-speed region (as depicted in Fig. 2), (13) can be correspondingly transformed into

$$\omega_m^c(t) = (1.5p_nK_ec_1 - C^+)\big/B_h^+. \tag{14}$$

The above equation reveals that if different constant currents that can make the final steady open-loop speed response fall within the high-speed region are injected into the q-axis, then the induced open-loop speed responses will eventually stabilize at constant values that depend solely on the magnitude of the injected current. This conclusion will be used for the determination of C^+. Further analysis is as follows.

In (14), both the injected current c_1 and the final steady open-loop speed response values are known so that this equation only contains two unknowns, i.e., C^+ and B_h^+. Consequently, calculating the value of C^+ needs two independent equations, i.e., two distinct constant q-axis current injections are required. Assuming that the two injected currents that make the final steady open-loop speed response fall within the high-speed region are c_{1_1} and c_{1_2}, and final stabilized speed response values are ω_{m1} and ω_{m2}, one has

$$\begin{cases} B_h^+\omega_{m1} = 1.5p_nK_ec_{1\_1} - C^+ \\ B_h^+\omega_{m2} = 1.5p_nK_ec_{1\_2} - C^+. \end{cases} \tag{15}$$

Thus, solving (15) yields the calculation formula for C^+:

$$\begin{cases} \hat{C}^+ = (1.5p_nK_ec_{1\_2}\omega_{m1} - 1.5p_nK_ec_{1\_1}\omega_{m2})\big/(\omega_{m1} - \omega_{m2}) \\ \hat{B}_h^+ = (1.5p_nK_ec_{1\_1} - 1.5p_nK_ec_{1\_2})\big/(\omega_{m1} - \omega_{m2}) \end{cases} \tag{16}$$

where $\hat{C}^+$ and $\hat{B}_h^+$ are the identified values of C^+ and B_h^+, respectively. Similarly, we can derive the calculation formula for C^- as follows:

$$\begin{cases} \hat{C}^- = (1.5p_nK_ec_{1\_3}\omega_{m4} - 1.5p_nK_ec_{1\_4}\omega_{m3})\big/(\omega_{m3} - \omega_{m4}) \\ \hat{B}_h^- = (1.5p_nK_ec_{1\_3} - 1.5p_nK_ec_{1\_4})\big/(\omega_{m3} - \omega_{m4}) \end{cases} \tag{17}$$

where $\hat{C}^-$ and $\hat{B}_h^-$ are the identified values of C^- and B_h^-, respectively; c_{1_3}, c_{1_4}, ω_{m3}, and ω_{m4} refer to the corresponding injection currents and final stabilized speed response values, respectively. With (16) and (17), C^+ and C^- can be determined.

From the above analysis, it is evident that selecting appropriate constant injection currents is crucial for accurately determining

C^+ and C^-. Given that the viscous friction coefficient in the high-speed region, B_h^+ or B_h^-, is constant, this paper designs a simple procedure to automatically search/determine the appropriate constant injection currents, as shown in Fig. 3. The complete algorithmic details for Routine I and Routine II of Fig. 3 are provided in Appendix. It should be noted that Fig. 3 only illustrates the principle of the automatic search procedure for the constant injection currents used to calculate C^+. For the calculation process of C^-, the procedure remains identical except for replacing the calculation formula (16) with (17) and randomly setting the initial value of i_q^{in} (i.e., the initial i_{val}) in the range $-I_N$ to 0 (I_N is the rated current). As shown in Fig. 3, the developed procedure determines the appropriate constant injection current through two phases (i.e., rough search and fine search phases), and then utilizes (16) to achieve the precise identification of C^+. The rough search phase aims to quickly lock onto a reasonable injection current range, which contains suitable injection currents that can make the final steady open-loop speed response fall within the high-speed region. The subsequent fine search phase gradually determines the appropriate injection currents in an iteration manner. When the calculated B_h^+ remains essentially constant (i.e., satisfying the final judgment condition "$|(\text{rc3}-\text{rc4})/\text{rc4}| \le 1\%$" and triggering the command "$i_q^{\text{in}} = 0$" in Routine II), the currently identified C^+ can be deemed as the desired value.

2) Speed-Decay-Based Identification of the Initial Inertia: Identifying the initial inertia aims to lay the groundwork for subsequent viscous friction coefficient estimation and speed controller self-tuning. Additionally, if the drive system's inertia remains unchanged during the work operation, the identified initial inertia value can be directly used as the final inertia estimation result.

Remark 1: The speed controller self-tuning can be easily attained with the aid of the inertia value [21], i.e.,

$$\begin{cases} K_P = J\omega_c / k_t \\ K_I = J\omega_c^2 / (5k_t) \end{cases} \tag{18}$$

where $k_t = 1.5 p_n K_e$; K_P and K_I are the proportional and integral gains of the speed controller, respectively; ω_c is the desired closed-loop bandwidth of the speed controller.

The identification of the initial inertia is elaborated as follows. When a q-axis current is injected to drive the motor to its allowable maximum speed, the motor will undergo a natural speed decay process until reaching zero if the injected q-axis current signal is abruptly discontinued (i.e., $i_q^{\text{in}} = 0$). This paper determines the initial inertia by utilizing the high-speed region data from the open-loop speed response triggered by natural decay. Next, take (8) as an example for further analysis. Prior to the drive system's work operation, let us define the initial inertia as J_{init}. Hence, based on (8), one has

$$J_{\text{init}}\dot{\omega}_m = T_e - B^+\omega_m - C^+. \tag{19}$$

Then, the following result can be obtained.

Theorem 2: If the initial inertia of the PMSM drive system is defined as J_{init}, then in the high-speed region, the open-loop speed response induced by natural decay satisfies the following equation:

$$\ln[\omega_m^h(t) + C^+/B_h^+] = \ln(\omega_{m\_\max} + C^+/B_h^+) - (B_h^+/J_{\text{init}})t \tag{20}$$

where $\omega_m^h(t)$ denotes the natural-decay open-loop speed response in the high-speed region.

Proof: During the natural speed decay, the electromagnetic torque vanishes with zero q-axis current injection. Accordingly, (19) is simplified to

$$J_{\text{init}}\dot{\omega}_m^{nd} = -B^+\omega_m^{nd} - C^+ \tag{21}$$

where ω_m^{nd} stands for the natural-decay open-loop speed response.

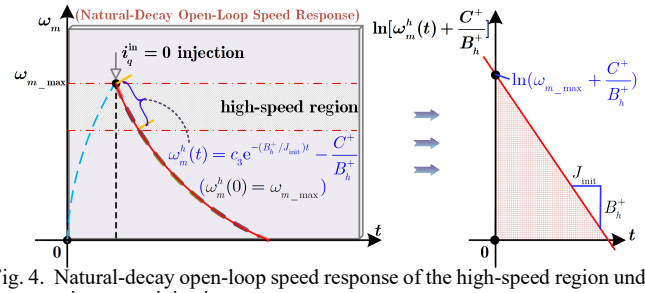

Fig. 4. Natural-decay open-loop speed response of the high-speed region under zero q-axis current injection.

As a result, in the high-speed region, one can rewrite (21) as

$$J_{\text{init}}\dot{\omega}_m^h = -B_h^+\omega_m^h - C^+. \tag{22}$$

Then, the analytic expression of (22) can be derived as

$$\omega_m^h(t) = e^{-\int \frac{B_h^+}{J_{\text{init}}}dt}\left[c_3 + \int(-\frac{C^+}{J_{\text{init}}})e^{\int \frac{B_h^+}{J_{\text{init}}}dt}dt\right] = c_3 e^{-\frac{B_h^+}{J_{\text{init}}}t} - \frac{C^+}{B_h^+} \tag{23}$$

where c_3 is a constant. If the starting moment of the natural speed decay is designated as the initial time point, we have $\omega_m^h(0) = \omega_{m\_\max}$. Thus, $c_3 = \omega_{m\_\max} + C^+/B_h^+$ (note that C^+ and B_h^+ have been previously calculated). Then, (23) can be rewritten as

$$\omega_m^h(t) + C^+/B_h^+ = (\omega_{m\_\max} + C^+/B_h^+)e^{-(B_h^+/J_{\text{init}})t}. \tag{24}$$

Taking the natural logarithm on both sides of (24) obtains

$$\begin{aligned} \ln[\omega_m^h(t) + C^+/B_h^+] &= \ln\left[(\omega_{m\_\max} + C^+/B_h^+)e^{-(B_h^+/J_{\text{init}})t}\right] \\ &= \ln(\omega_{m\_\max} + C^+/B_h^+) - (B_h^+/J_{\text{init}})t. \end{aligned} \tag{25}$$

This finishes the proof. Fig. 4 presents the schematic principle of deriving (25) from the natural-decay open-loop speed response.

Theorem 2 indicates that in the high-speed region, the natural-decay open-loop speed response can be transformed into a straight-line equation with a slope of $-B_h^+/J_{\text{init}}$ through logarithmic operations. Since B_h^+ has been previously determined during the Coulomb friction coefficient identification, the initial inertia value can be directly calculated by simply acquiring the slope of this straight line. Assuming the acquired slope is L_{slope}, the initial inertia value can be calculated as

$$\hat{J}_{\text{init}} = -\hat{B}_h^+/L_{\text{slope}} \tag{26}$$

where $\hat{J}_{\text{init}}$ is the identified value of J_{init}. Additionally, it merits mention that the two stabilized speed response values used for the final calculation of C^+ (denoted as s_1 and s_2), which are obtained during the execution of the automatic search procedure shown in Fig. 3, enable the rapid and accurate calculation of the slope. Specifically, in the logarithmic data calculated using the natural-decay speed response, the correct slope can be directly computed by applying a linear function to fit the data segment corresponding to the speed interval between s_1 and s_2.

3) Open-Loop Identification of the Viscous Friction Coefficient Varying with Speed: Given that the allowable maximum speed is defined as $\omega_{m\_\max}$, the speed domain of the drive system can be regarded as $[-\omega_{m\_\max}, \omega_{m\_\max}]$. In this paper, by utilizing the natural-decay open-loop speed response data and the previously identified parameters (i.e., the Coulomb friction coefficient and initial inertia), the viscous friction coefficient corresponding to each speed across the entire speed domain can be determined, i.e., identifying the viscous friction coefficient varying with speed is attained. Here, the detailed identification of B^+ is first introduced based on (21).

Substituting the estimated J_{init} and C^+ into (21) yields

$$\hat{B}^+ = (-\hat{J}_{\text{init}}\dot{\omega}_m^{nd} - \hat{C}^+)/\omega_m^{nd} \tag{27}$$

where $\hat{B}^+$ stands for the identified value of B^+.

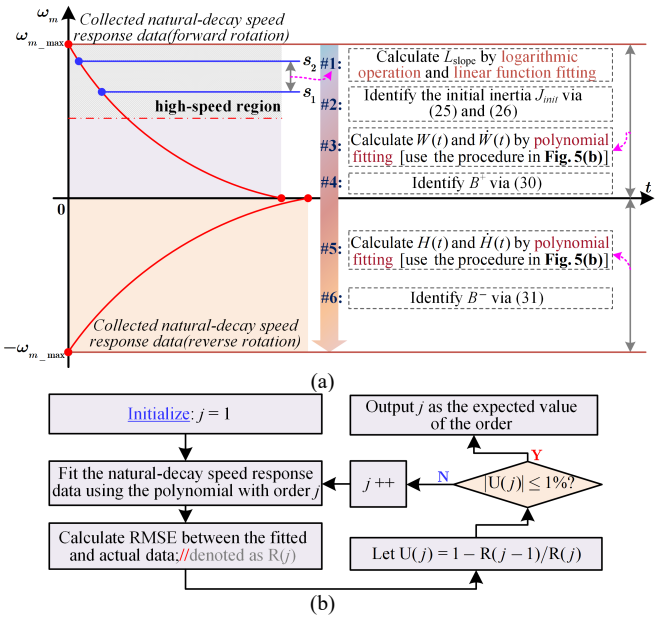

Fig. 5. Detailed flowchart of identifying the initial inertia and the viscous friction coefficient varying with speed. (a) Automatic implementation process. (b) Automatic determination of polynomial order.

Utilizing (27) and the speed response data, one can determine B^+. It should be noted, however, that (27) contains the differentiation of the speed response ω_m^{nd}. Clearly, performing the direct differentiation operation inevitably degrades the identification accuracy, as the speed data in practical applications is typically contaminated by noise. To address this concern, this paper employs a polynomial to fit ω_m^{nd}, avoiding direct differentiation. Assuming the fitting result of the natural-decay speed response ω_m^{nd} as $W(t)$, we have

$$\omega_m^{nd} = W(t) = w_f t^f + w_{f-1} t^{f-1} + \cdots + w_1 t + w_0 \tag{28}$$

where $w_i (i = 0,1,\cdots,f-1,f)$ stands for the fitting coefficient; f denotes the order of $W(t)$.

Differentiating $W(t)$ with respect to the time t yields

$$\dot{\omega}_m^{nd} = \dot{W}(t) = w_f t^{f-1} + w_{f-1} t^{f-2} + \cdots + w_1. \tag{29}$$

As a consequence, (27) can be rewritten as

$$\hat{B}^+ = (-\hat{J}_{\text{init}} \dot{W}(t) - \hat{C}^+) \big/ W(t). \tag{30}$$

Similarly, the identification formula for B^- can be expressed by

$$\hat{B}^- = (-\hat{J}_{\text{init}} \dot{H}(t) + \hat{C}^-) \big/ H(t) \tag{31}$$

where $\hat{B}^-$ is the identified value of B^-; $H(t)$ is the fitting result of the natural-decay open-loop speed response corresponding to the reverse motor rotation, and $H(t)$ and its derivative $\dot{H}(t)$ can be given by

$$\begin{cases} H(t) = h_r t^r + h_{r-1} t^{r-1} + \cdots + h_1 t + h_0 \\ \dot{H}(t) = h_r t^{r-1} + h_{r-1} t^{r-2} + \cdots + h_1 \end{cases} \tag{32}$$

where $h_i (i = 0,1,\cdots,r-1,r)$ stands for the fitting coefficient and r refers to the order of $H(t)$.

From the above analysis, it can be noticed that J_{init} and B are both identified based on the natural-decay open-loop speed response. To simplify the implementation, this paper develops an automatic process for identifying J_{init} and B by using the natural-decay speed response, as shown in Fig. 5. In this automatic process, the linear function used to calculate J_{init} can be automatically generated using the speed response data between s_1 and s_2. (i.e., the slope L_{slope} is automatically obtained). In addition, the appropriate order of the fitting polynomials $W(t)$ and $H(t)$ used for identifying B^+ and B^- can also be acquired with an automatic determination technique (its working principle is illustrated in Fig. 5(b)).

Remark 2: For the polynomial fitting, the fitting error typically decreases as the polynomial order increases, but when the order exceeds a certain critical value, the error will tend to stabilize [27]. Further increasing the order beyond this critical value will lead to higher computational costs and even overfitting. Consequently, Fig. 5(b) designs a simple technique for automatically determining the polynomial order, which uses the relative change rate of root mean square error (RMSE) as the criterion for choosing a suitable polynomial order.

Remark 3: From Fig. 3 and Routine II of the Appendix, we can notice that at the end of the fine search phase, the condition $|\omega_m| \geq \omega_{m\_\max}$ will be satisfied, and the command $i_q^{\text{in}} = 0$ will be triggered simultaneously. Thus, the natural-decay open-loop speed response can be obtained without the need for an additional test.

B. Identification of Step II (Speed Loop Closed)

As previously mentioned, the identification process in Step I is executed before the PMSM system is put into the work operation. When the drive system transitions into its work phase, the load torque is typically present, and furthermore, both the load torque and inertia may be time-varying. In this paper, an innovative online algebraic estimator is developed for the precise tracking of time-varying load torque and inertia, managing such a challenge.

Based on the mechanical motion model (3), we have

$$J\dot{\omega}_m = T_e^l - T_L \tag{33}$$

where T_e^l is given by

$$T_e^l = \begin{cases} T_e - B^+\omega_m - C^+, & (\omega_m > 0) \\ T_e, & (\omega_m = 0) \\ T_e - B^-\omega_m + C^-, & (\omega_m < 0). \end{cases} \tag{34}$$

It should be noted that since the values of B^+, C^+, B^-, and C^- have already been determined, T_e^l in (34) can be directly calculated using real-time measurements/calculations of ω_m and i_q.

When both sides of (33) are multiplied by the time t and integrated over the interval $[0,t]$, it follows that

$$\int_0^t tJ\dot{\omega}_m = \int_0^t tT_e^l - \int_0^t tT_L. \tag{35}$$

In general, the change frequency for both the inertia and load torque is much lower than the switching frequency of the PMSM system. Therefore, it is reasonable to assume that these two parameters remain nearly constant over a short time interval. Accordingly, during a short time interval, (35) can be rewritten as

$$\int_0^t tT_e^l = J(t\omega_m - \int_0^t \omega_m) + 0.5T_L t^2. \tag{36}$$

Then, (36) can be reformulated in the regressor form as follows:

$$Q(t) = P(t)\Theta \tag{37}$$

where $Q(t) = \int_0^t tT_e^l$; $P(t) = [(t\omega_m - \int_0^t \omega_m) \quad t^2/2]$; $\Theta = [J \quad T_L]^T$, which is the to-be-identified unknown vector.

To solve (37), this paper establishes a set of linearly independent equations by formulating the identification of the unknown vector Θ as an optimization problem. First, we construct the following equation as the cost function, serving as the optimization criterion:

$$L(\hat{\Theta}, t) = \frac{1}{2}\int_0^t e^2(\hat{\Theta}, \sigma)\mathrm{d}\sigma \tag{38}$$

where $e(\hat{\Theta}, \sigma) = P(\sigma)\hat{\Theta} - Q(\sigma)$. Here, $\hat{\Theta} = [\hat{J} \quad \hat{T}_L]^T$, where $\hat{T}_L$ and $\hat{J}$ refer to the identified values of T_L and J, respectively. Therefore, the optimization problem can be stated as

$$\min_{\hat{\Theta}} L(\hat{\Theta}, t) = \min_{\hat{\Theta}} \frac{1}{2}\int_0^t [P(\sigma)\hat{\Theta} - Q(\sigma)]^2 \mathrm{d}\sigma. \tag{39}$$

Differentiating $L(\hat{\Theta}, t)$ with respect to $\hat{\Theta}$ yields

$$\begin{aligned} \nabla_{\hat{\Theta}} L(\hat{\Theta}, t) &= \frac{\partial}{\partial \hat{\Theta}} \frac{1}{2}\int_0^t e^2(\hat{\Theta}, \sigma) = \int_0^t \frac{\partial e}{\partial \hat{\Theta}} e(\hat{\Theta}, \sigma)\mathrm{d}\sigma \\ &= \int_0^t P^T(\sigma)[P(\sigma)\hat{\Theta} - Q(\sigma)]\mathrm{d}\sigma. \end{aligned} \tag{40}$$

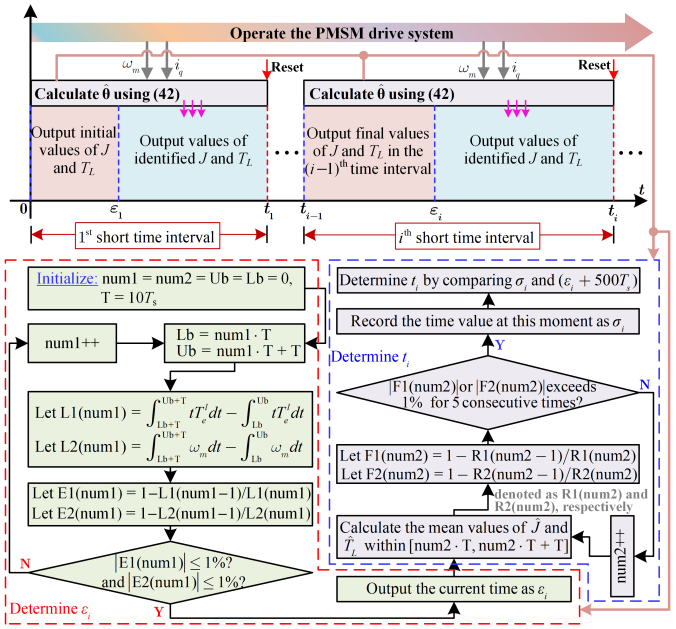

Fig. 6. Detailed implementation mechanism of the proposed online algebraic estimator.

From (38), we can notice that $L(\hat{\Theta},t)$ is a convex function, so it has a global minimum when $\nabla_{\hat{\Theta}}L(\hat{\Theta},t)=0$. Consequently, one has

$$\left[\int_0^t P^T(\sigma)P(\sigma)\mathrm{d}\sigma\right]\hat{\Theta}=\int_0^t P^T(\sigma)Q(\sigma)\mathrm{d}\sigma. \tag{41}$$

As a result, $\hat{\Theta}$ can be expressed as follows:

$$\hat{\Theta}=\left[\int_0^t P^T(\sigma)P(\sigma)\mathrm{d}\sigma\right]^{-1}\int_0^t P^T(\sigma)Q(\sigma)\mathrm{d}\sigma. \tag{42}$$

Given that T_L and J are considered to potentially vary over time during the work operation of the drive system, (42) needs to reset its parameter calculations at the end of each short time interval. Additionally, considering that the integral term is highly susceptible to measurement noise during the initial stage of integration, it is essential to retain the final calculated value of the previous time interval for a short duration after each reset, until the integral term has sufficiently grown to mitigate the influence of noise. Hence, within the i^{th} short time interval, $\hat{\Theta}$ can be calculated as

$$\hat{\Theta}_i(t)=\begin{cases}\hat{\Theta}_{i-1}(t_{i-1}),(t_{i-1}\le t\le \varepsilon_i)\\ \left[\int_{t_{i-1}}^t P^T(\sigma)P(\sigma)\mathrm{d}\sigma\right]^{-1}\int_{t_{i-1}}^t P^T(\sigma)Q(\sigma)\mathrm{d}\sigma,(\varepsilon_i<t\le t_i)\end{cases} \tag{43}$$

where $\hat{\Theta}_i$ and $\hat{\Theta}_{i-1}$ stand for the identified vector in the i^{th} and $(i-1)^{th}$ short time interval, respectively; ε_i refers to the short duration at the initial calculation stage of the i^{th} short time interval; t_{i-1} and t_i are the reset time points of the $(i-1)^{th}$ and i^{th} short time interval, respectively (i.e., the length of the i^{th} short time interval is t_i-t_{i-1}). Note that during the first short time interval (i.e., when $t\le t_1$), C^+ and J_{init} identified in Step I can be used as the output values of $\hat{T}_L$ and $\hat{J}$ within the time span of ε_1.

In practical applications, the values of ε_i and t_i at the i^{th} short time interval can be adaptively determined based on the actual characteristics of the operating condition or the drive system. Fig. 6 shows the detailed identification process and practical implementation mechanism of the proposed online algebraic estimator. The principles for determining ε_i and t_i in Fig. 6 are further explained as follows:

i) Determination of ε_i: As mentioned above, the integral term in the initial stage of integration is significantly affected by noise. However, as the integration time increases, the contribution of noise to the integral term will tend to be gradually smoothed due to the low-pass filtering effect of the integration. This causes the absolute variation of the integral term over the same time span to move toward consistency. Based on this characteristic, this paper uses the change rate of the absolute variation in some key integral terms (i.e., the terms $\int_0^t tT_e^l$ and $\int_0^t \omega_m$ in (37)) as the criterion to evaluate whether the integral term has grown sufficiently. When the change rate of the absolute variation remains almost constant (i.e., the absolute variation of the integral term tends to stabilize), the integral term can be considered to have grown sufficiently. The time value at this point can be deemed as ε_i.

ii) Determination of t_i: According to (35), we can notice that if parameter calculation resets are not performed, the identified values are essentially weighted averages over the entire integration interval. When the actual parameters change over time, the identification results will also vary, even though they cannot accurately reflect the variations of the actual parameters due to the weighted averaging effect of integration. Therefore, in practical implementation, the relative change rate of the identification results' averages can be used as the criterion to evaluate whether the actual parameters have changed, thereby determining the reset time t_i in real time. For instance, when the means of multiple identification results continuously increase, it can be considered that the actual parameters have changed. Suppose the time at which the criterion is met during the i^{th} short time interval is σ_i, then $t_i=\sigma_i$. For cases where the criterion is not met (e.g., the actual parameters remain constant), a fixed period of ε_i+500T_s (T_s is the speed-loop sampling period, which satisfies $T_s=0.0002$ s in this paper) is set for resetting, so as to prevent the integration from becoming unbounded. Overall, the value of t_i can be expressed as $t_i=\min\{\sigma_i,\varepsilon_i+500T_s\}$.

Remark 4: From the above analysis, it is easy to notice that the maximum value of t_i can only be taken as ε_i+500T_s (which is $\varepsilon_i+0.1$ in this paper). Further clarification regarding ε_i+500T_s is provided below. In practical applications, algebraic identification is able to obtain true values almost instantaneously [23], which suggests that once the integration begins, the noise will be rapidly smoothed and suppressed. As a result, ε_i usually tends toward a very small value, thereby resulting in ε_i+500T_s being generally on the millisecond scale. Thus, even if t_i is assigned the value of ε_i+500T_s in some special cases, a millisecond-level reset time is more than adequate for most engineering application scenarios where the load torque and inertia are time-varying.

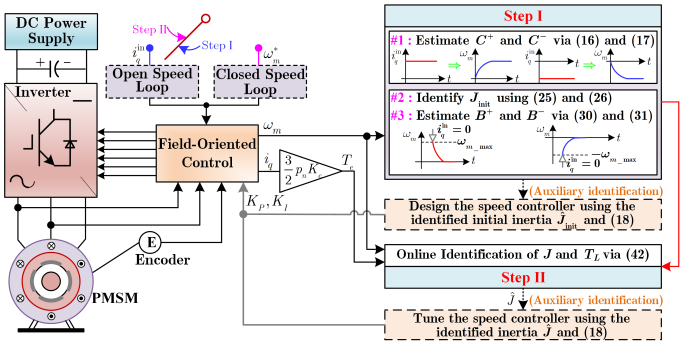

Fig. 7. Overall schematic diagram of the proposed method.

C. Brief Summary

Fig. 7 illustrates the overall schematic diagram of the proposed parameter-tuning-free two-step MPI method. As shown, the proposed method consists of two collaborative steps along with their auxiliary identification components related to the speed controller self-tuning. The detailed identification process of two steps has been described in Section III-A and Section III-B. Step I

is conducted prior to the drive system's work operation. Through signal injections under the open-loop condition of the speed loop, this step enables the identification of the Coulomb friction coefficient, the initial inertia, and the viscous friction coefficient varying with speed. It should be emphasized that the successful execution of this step implies the attainment of automatic nonlinear friction modeling. Step II is performed during the drive system's work operation and operates under closed-loop speed control. It leverages the developed algebraic estimator and the identification results from Step I to acquire the inertia and load torque simultaneously and in real time.

The parameter-tuning-free characteristic of our proposed method is reflected in the fact that it involves neither adjusting any of its own parameters nor tuning the speed controller. Here, further explanation is provided for the latter. First, since Step I is conducted with the speed loop opened, the speed controller's parameter adjustment is naturally unnecessary. In Step II, the initial inertia identified in Step I is used to adjust the speed controller, enabling it to initially have normal closed-loop operation ability. Subsequently, during the online identification of inertia and load torque, the estimated inertia is used to tune the speed controller in real time (i.e., identification and controller tuning are performed simultaneously), preventing the speed controller from malfunctioning due to inertia mismatch. Overall, Step II is automatically capable of tuning the speed controller, avoiding the workload associated with manual parameter design.

Remark 5: After completing Step I, the identification result of the viscous friction coefficient varying with speed can be used to construct a lookup table. Then, during Step II and the actual application of the estimated B^+ and B^-, the matching viscous friction coefficient value can be determined online based on the real-time speed.

Remark 6: In practice, friction conditions typically undergo slow changes over time due to factors such as wear-induced aging and lubricant consumption. Consequently, the Coulomb and viscous friction coefficient may exhibit the slow time-varying characteristic. To cope with such an issue, Step I can be periodically re-executed to update these two friction coefficients.

Remark 7: Although the proposed method is designed for PMSM systems under the framework of FOC with $i_d^* = 0$, it can be easily extended to the maximum torque per ampere (MTPA)-based PMSM system. In fact, compared to the FOC with $i_d^* = 0$, the MTPA control essentially only adds an optimal *dq*-axis current command calculation module. To implement Step I under the MTPA control framework, one only needs to set the *d*-axis current command i_d^* to zero, while directly injecting the same current command signals as in this paper into the *q*-axis. As for Step II, its implementation only requires the drive system to provide real-time information on ω_m and T_e, regardless of the adopted control strategy. Given that surface-mounted PMSMs typically adopt the FOC with $i_d^* = 0$ and interior PMSMs widely apply the MTPA control, the above analysis indicates that the proposed method is applicable to both surface-mounted and interior PMSMs.

IV. Experimental Investigations

A. System Setup

The experimental system for validating the proposed method, shown in Fig. 8, is composed of three primary components: 1) a host computer for code debugging/programming, signal monitoring, and test data collection/storage/processing; 2) a motor driver built based on an STM32F407 microcontroller (168-MHz CPU/210 DMIPS); 3) an algorithm validation platform integrating a 1.2-kW prototype PMSM, a high-precision torque sensor, a 1.2-kW load motor serving as a programmable load torque source, and a dedicated load motor driver. The detailed specifications of the experimental system are summarized in Table I. In addition,

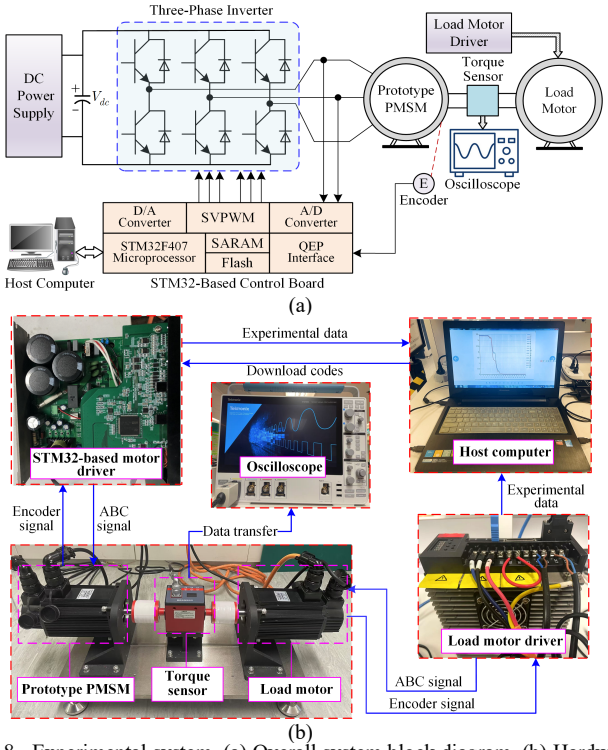

Fig. 8. Experimental system. (a) Overall system block diagram. (b) Hardware photograph.

TABLE I
DETAILED SPECIFICATIONS OF THE EXPERIMENTAL SYSTEM

Parameters		Values/Units
DC bus voltage		310 V
PWM's switching frequency		10 kHz
Encoder resolution (incremental)		2500 p/r
Total inertia		0.00229 kg·m^2
Prototype PMSM	Rated current	6 A
	Rated torque	6 N·m
	Rotor inertia	0.001111 kg·m^2
	Stator resistance	0.64 Ω
	q-axis inductance	2.764 mH
	d-axis inductance	2.764 mH
	Number of pole pairs	4

the FOC strategy with $i_d^* = 0$ (as depicted in Fig. 1) is applied to control the prototype PMSM, while the load motor operates in torque control mode.

B. Experimental Tests

1) Identification of Step I: Here, some tests concerning Step I of our proposed method are conducted to identify the Coulomb friction coefficient, the initial inertia, and the viscous friction coefficient varying with speed. First, the automatic search procedure illustrated in Fig. 3 is executed to determine appropriate constant injection currents and, meanwhile, to calculate C^+ and C^-. Figs. 9(a) and 9(b) show the relevant experimental outcomes obtained during the execution of this procedure. From there, it can be observed that through the rough search (executing Routine I) and the fine search (executing Routine II), the command "$i_q^{\text{in}} = 0$" is triggered by the designed automatic search procedure. This indicates that the final judgment condition "$|(\text{rc3} - \text{rc4})/\text{rc4}| \le 1\%$" set in Routine II has been satisfied (i.e., the calculated B_h remains almost constant), thereby implying that suitable constant *q*-axis injection currents have been found to make the generated final steady speed responses fall within the high-speed region. The experimental phenomenon, i.e., the values of $\hat{B}_h$ that are calculated using the final stabilized speed response values induced by the last few constant-current injections remain almost unchanged, confirms the above conclusion. From Figs. 9(a) and

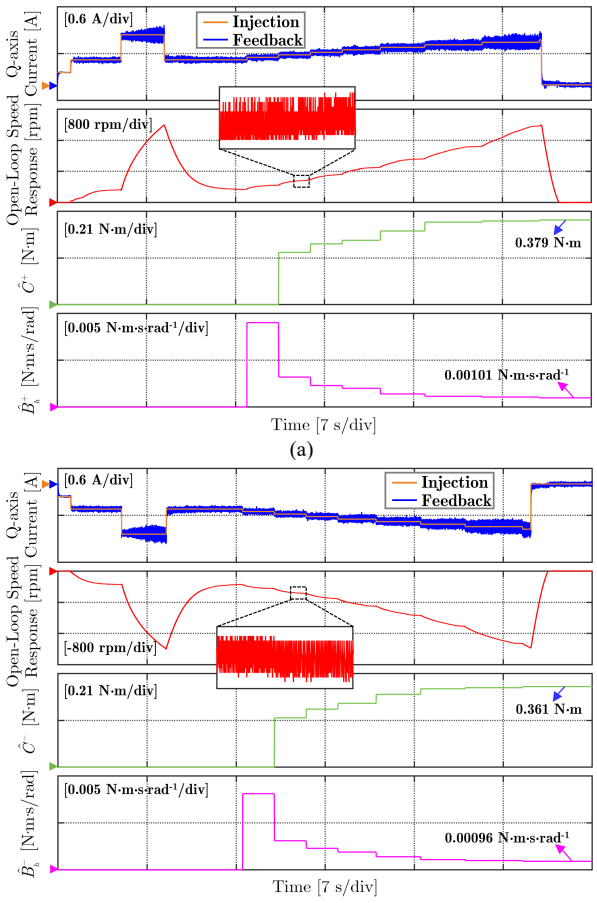

Fig. 9. Identification of C^+, C^-, B_h^+, and B_h^-. (a) Identifying C^+ and B_h^+. (b) Identifying C^- and B_h^-.

9(b), one can see that the estimated C^+ and B_h^+ are 0.379 N·m and 0.00101 N·m·s·rad^{-1}, respectively, while their counterparts C^- and B_h^- are identified as 0.361 N·m and 0.00096 N·m·s·rad^{-1}.

As pointed out in Remark 3, the natural-decay open-loop speed responses under the forward and reverse motor rotation can be directly obtained from Figs. 9(a) and 9(b). With these two natural-decay speed responses and by following the implementation process shown in Fig. 5, the linear function fitting result of $\ln(\omega_{m\_\max} + C^+/B_h^+) - (B_h^+/J_{\text{init}})t$, as well as the fitting polynomials $W(t)$ and $H(t)$, can be obtained, thereby enabling the calculation of the initial inertia, B^+, and B^-. Fig. 10(a) depicts the natural-decay speed response over the speed domain $[0,\ \omega_{m\_\max}]$ and the corresponding calculation result of $\ln[\omega_m^{nd} + C^+/B_h^+]$, while the fitted result of $\ln(\omega_{m\_\max} + C^+/B_h^+) - (B_h^+/J_{\text{init}})t$ is given in Fig. 10(b). According to this fitting result, one has $L_{\text{slope}} = -0.4346$. As a result, the initial inertia can be calculated as $\hat{J}_{\text{init}} = 2.324 \times 10^{-3}$ kg·m^2 (only about 1.48% error). Similarly, during the execution of the implementation process shown in Fig. 5, the related experimental results presented in Fig. 10(c) can also be yielded. By using the fitting polynomial results obtained from Fig. 10(c) and the previously determined $\hat{J}_{\text{init}}$, $\hat{C}^+$, and $\hat{C}^-$, the identification results of B^+ and B^- can be derived, as shown in Fig.10(d).

2) Identification Accuracy Assessment of Step I: To evaluate the accuracy of the identified parameters $\hat{C}^+$, $\hat{C}^-$, $\hat{J}_{\text{init}}$, $\hat{B}^+$, and $\hat{B}^-$, a validation test is conducted comprising the following steps: *i*) inject a random *q*-axis current command with the speed loop opened; *ii*) acquire the actual data of i_q and ω_m during the injection; *iii*) substitute the identified parameters and the acquired *q*-axis current data into (8) and (9) to compute the

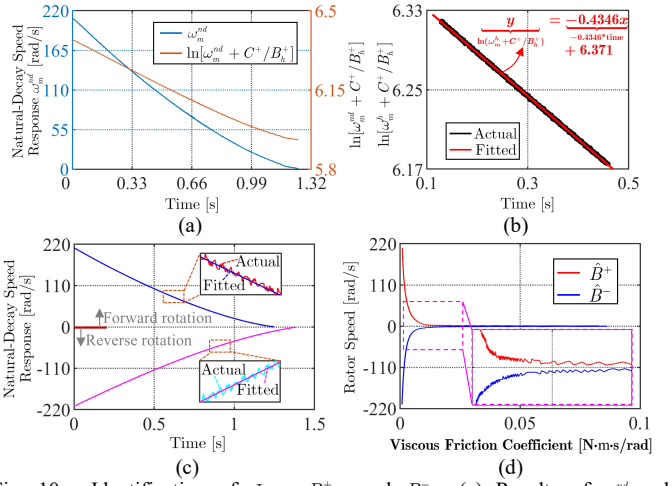

Fig. 10. Identification of J_{init}, B^+, and B^-. (a) Results of ω_m^{nd} and $\ln(\omega_m^{nd} + C^+/B_h^+)$. (b) Linear function fitting of natural-decay speed response in the high-speed region. (c) Polynomial fitting of natural-decay speed responses under forward and reverse rotation. (d) Identified B^+ and B^-.

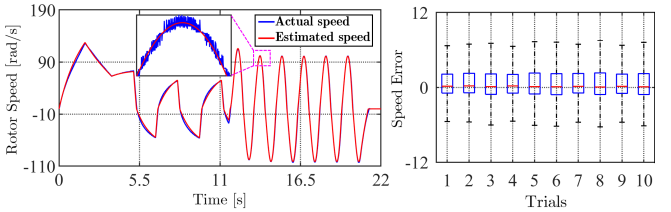

Fig. 11. Accuracy verification test. (a) Comparison of the estimated and actual speeds. (b) Boxplot of the speed error for ten repeated trials.

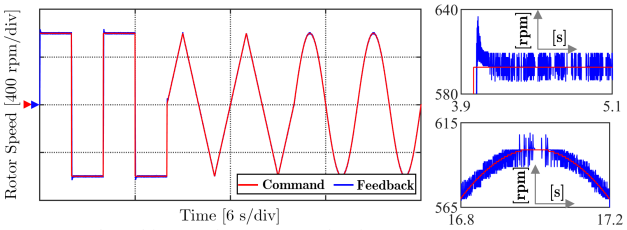

Fig. 12. Speed tracking performance evaluation.

estimated speed; *iv*) compare the actual speed with the estimated speed to assess the accuracy. Fig.11(a) presents the comparison between the actual and estimated speed. As evident from there, the estimated speed aligns well with the actual one, which indicates the identified parameters possess high accuracy. To enhance the validity, ten repeated experiments are performed. Fig. 11(b) offers the quantitative analysis of repeated test results by plotting the boxplot. The result reveals that the identification outcomes exhibit good consistency and stability among these repeated tests, which strongly supports the reliability of the above conclusion.

3) Design and Performance Evaluation for the Speed Controller: Based on the estimated initial inertia, the speed controller can be designed using (18), enabling it to initially possess a normal closed-loop operation capability. Fig. 12 shows the speed tracking responses of the experimental platform under various references (note that the desired bandwidth ω_c is 20 rad/s). The experimental results demonstrate that the designed speed controller is not only stable but also capable of achieving high-precision speed tracking. This lays a solid foundation for the implementation of Step II. It merits mention that, considering the potential inertia variations of the drive system during task execution, the online-identified inertia in Step II will be utilized to update the speed controller's parameters in real time.

4) Identification of Step II (Performance Evaluation of Step II Under Different Operating Conditions): Here, Step II of our developed approach is experimentally tested under

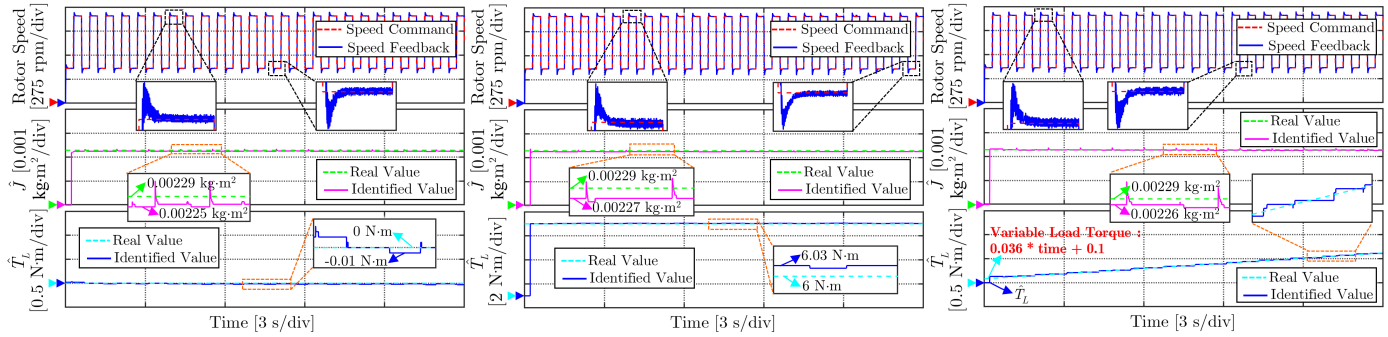

Fig. 13. Performance tests of the proposed online algebraic estimator under various load conditions. (a) No-load. (b) 6-N·m constant load. (c) Time-varying load.

TABLE II
COMPARISON OF EXISTING METHODS WITH OUR PROPOSED APPROACH

Comparison Methods		Mechanical Parameters That Can Be Identified				Method Characteristics			
		J	B	C	T_L	Friction Asymmetry	Friction Nonlinearity	Can both J and T_L be identified online?	Parameter Tuning
Existing Methods	Zhang and Li [12]	✓	✓	Treated as a lumped parameter		Ignored	Ignored	Unable	Required
	Kim [21]	✓	✓	✓	×	Ignored	Ignored	Unable	Required
	Lian *et al.* [14]	✓	Treated as a lumped parameter		✓	Ignored	Ignored	Able	Required
	Yang *et al.* [22]	✓	✓	✓	×	Ignored	Considered	Unable	Required
	Kobayashi *et al.* [13]	✓	✓	✓	×	Only considers the asymmetry of C	Ignored	Unable	Required
	Huang *et al.* [24]	✓	Treated as a lumped parameter		✓	Considered	Considered	Able	Required
	Yang *et al.* [4]	✓	✓	✓	✓	Ignored	Ignored	Able	Required
Proposed Method		✓	✓	✓	✓	Considered	Considered	Able	Not required

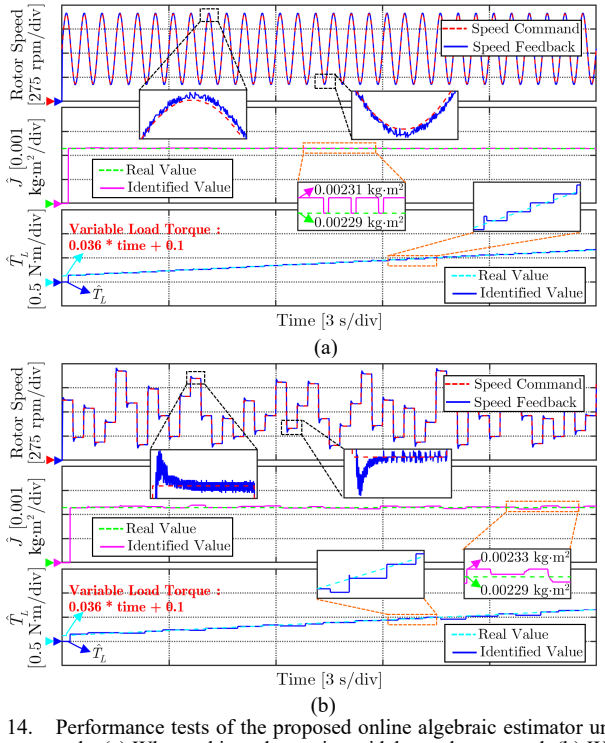

Fig. 14. Performance tests of the proposed online algebraic estimator under various speeds. (a) When subjected to a sinusoidal speed command. (b) When subjected to a random speed command.

different operating conditions to examine the online load torque and inertia identification performance of the designed algebraic estimator. First, Step II is evaluated under various load conditions. The corresponding test outcomes are depicted in Fig. 13. It is noted that during the experiments, the output values of T_L and J within the time span of ε_1 are both assigned to zero to highlight the proper functioning of the implementation mechanism shown in Fig. 6. In practical implementations, however, their output values within the time span of ε_1 can directly use the C^+ and J_{init} calculated in Step I, facilitating the effective utilization of the identified values. From Fig. 13, one can easily observe that the proposed online algebraic estimators can accurately track both T_L and J, regardless of whether no-load, constant load, or time-varying load conditions are applied. These test phenomena highlight the excellent identification performance of Step II, while also indirectly confirming that Step I has achieved the accurate identification.

Although the previous tests have yielded promising results under the square-wave speed reference, it is noteworthy that the real-world PMSM drive system may also encounter speed references that are sinusoidal, or even random and irregular. Fig. 14 presents the experimental results of Step II under sinusoidal and random speed commands. It is noted that the time-varying load torque, congruent with that in Fig. 13(c), is applied to the PMSM system during the test. It can be readily seen from Fig.14 that the proposed online algebraic estimator can accurately identify both T_L and J under the given sinusoidal and random command, further validating the effectiveness of the proposed method.

5) Performance Comparison With Previous Works: To fully evaluate the performance of our proposed method, several typical MPI methods, listed in Table II, are selected for comparative investigations. As evident from Table II, our method manifests more advantages over previously reported works. Here, the proposed method is first compared with the existing approaches [12], [13], [21], [22], and [24] in terms of the identification of J, B, and C. To visually present the comparison results, this paper follows the above-mentioned identification accuracy evaluation process, i.e., the identification results of these methods are substituted into their respective identification models to calculate the estimated speeds, which are then compared with the actual speed. The corresponding comparison results are shown in Fig. 15. From there, it can be seen that, compared with our method, these comparative methods yield estimated speeds with larger deviations from the actual speed. Moreover, the boxplot data and performance indicators, such as the coefficient of determination (denoted as R^2) and the RMSE, perform worse. Clearly, these test results indicate that the accuracy of our proposed method outperforms these comparison methods. This enhanced performance can be primarily attributed to the fact

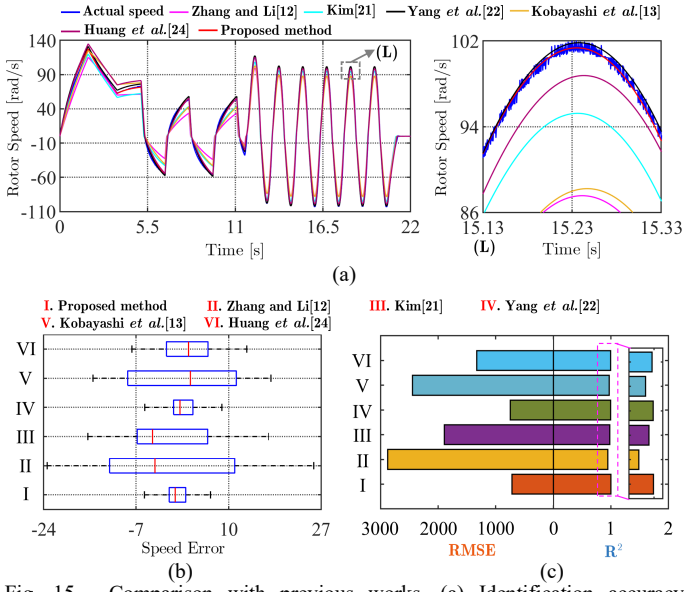

Fig. 15. Comparison with previous works. (a) Identification accuracy comparison. (b) Boxplot comparison. (c) Comparison of RMSE and R^2.

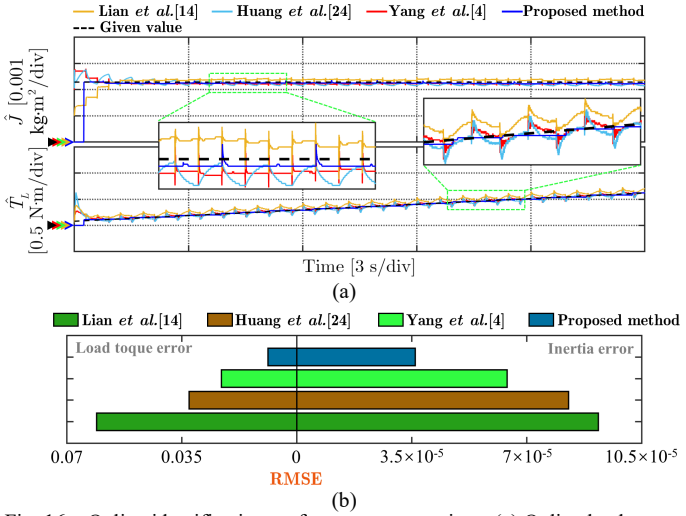

Fig. 16. Online identification performance comparison. (a) Online load torque and inertia identification results. (b) RMSE comparison of identification results in the time span [3, 9].

that the proposed method considers both the nonlinearity and asymmetry of friction.

Furthermore, this paper compares the proposed method with the existing methods [4], [14], and [24] in terms of online load torque and inertia identification performance under the time-varying load condition. The results shown in Fig. 16 indicate that our proposed method possesses more competitive accuracy in the real-time tracking of T_L and J, as evidenced by their smaller identification errors. Besides, on the STM32F407 microcontroller, the online execution time of these methods is compared with that of the proposed method, as shown in Fig. 17. It can be easily observed that the computational burden of the proposed method resides at a medium level, neither the lowest nor the highest. Notably, when compared to these contrastive methods, our proposed approach not only achieves superior accuracy (as shown in Fig. 16) but also successfully eliminates the need for parameter adjustments. Hence, it can be concluded that the proposed method exhibits more competitive advantages while imposing only a moderate computational burden.

6) A Control Effect Test Case: A simple application case concerning our developed method is provided to demonstrate the potential benefits stemming from the accurate identification of

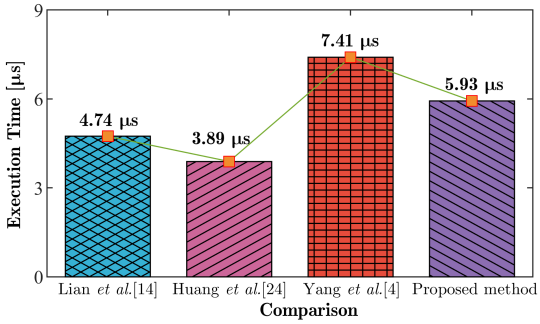

Fig. 17. Online execution time comparison.

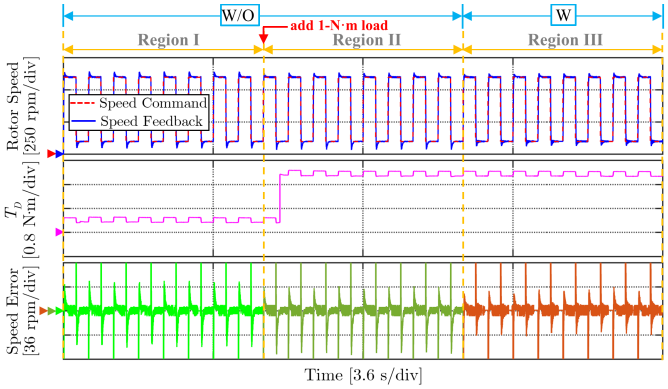

Fig. 18. Experimental result of the simple application case.

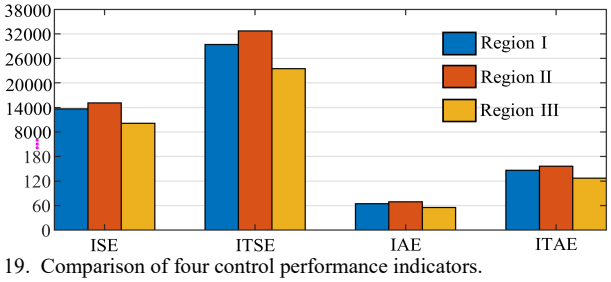

Fig. 19. Comparison of four control performance indicators.

mechanical parameters. In this application case, the identified load torque and friction coefficients are employed for feedforward compensation to seek to mitigate or counteract the effect of load variations and friction, improving the PMSM drive system's speed control performance. Consequently, in this case, the compensated q-axis current command can be calculated as $i_q^* = i_q^s + T_D/k_t$, where i_q^s stands for the output of the speed controller; T_D denotes the total disturbance torque, which can be expressed as $T_D = \hat{T}_L + \hat{C}^+ + \hat{B}^+\omega_m(\omega_m > 0)$ or $T_D = \hat{T}_L - \hat{C}^- + \hat{B}^-\omega_m(\omega_m < 0)$.

Fig. 18 presents the experimental results before and after feedforward compensation (note that "W" and "W/O" denote "with feedforward compensation" and "without feedforward compensation", respectively). As illustrated in Fig. 18, in Region I, the PMSM drive system is only subject to the friction torque, whereas in Regions II and III, a 1-N·m load torque is applied to the PMSM system. Moreover, feedforward compensation is activated in Region III. It is evident that a significant reduction in speed tracking error can be observed after accounting for load torque and friction compensation.

Furthermore, a comparison of four control performance indicators, including the integral square error (ISE), integral time square error (ITSE), integral absolute error (IAE), and integral time absolute error (ITAE), is presented in Fig. 19. From there, we can observe that these indicators exhibit a substantial improvement when feedforward compensation is activated (e.g., the ITSE indicator exhibits a decline exceeding 15% from Region II to Region III). This experimental result confirms that the PMSM

drive system employing our method possesses a good anti-disturbance capability.

It should be noted that this paper only explores a simple application case of the proposed method to highlight the potential significance of identifying mechanical parameters. Actually, our approach is capable of being applied to more control cases, including, but not restricted to, lubrication/wear assessment, controller tuning, fault monitoring, and optimization of nonlinear control (e.g., sliding-mode and predictive control).

V. Conclusion

In this work, a parameter-tuning-free two-step MPI method is proposed for the first time. By leveraging the open-loop speed response induced by signal injection and the algebraic estimator, the presented method enables the identification of the Coulomb friction coefficient, viscous friction coefficient varying with speed, inertia, and load torque under the consideration of friction nonlinearity and asymmetry. Additionally, this method is capable of effectively handling complex scenarios involving time-varying load torque and inertia. In contrast to previously reported MPI methods, the proposed approach stands out by requiring neither its own parameter adjustment nor speed controller parameter tuning. Moreover, its competitiveness is also underscored by superior identification accuracy. Extensive experiments conducted on a 1.2-kW PMSM system have validated the effectiveness of the presented method and demonstrated its superiority.

The proposed method promises to be widely deployed in typical variable-speed industrial applications, like machine tools, automated production lines, and robotic arms, thereby improving the operational quality and intelligence level. Besides, it merits mention that implementing our proposed approach demands the PMSM system to provide speed and electromagnetic torque information, which is indirectly obtained by position and current sensors. Our future work will focus on investigating how to achieve reliable identification of mechanical parameters under the sensor fault condition. Moreover, exploring more application cases concerning our method is also an important research direction.

Appendix

In Fig. 3, a simple procedure is designed to automatically search/determine the suitable constant injection currents. In the developed procedure, rough search and fine search phases are implemented by Routine I and Routine II, respectively. The specific algorithmic details for Routine I and Routine II are shown in Fig. 20.

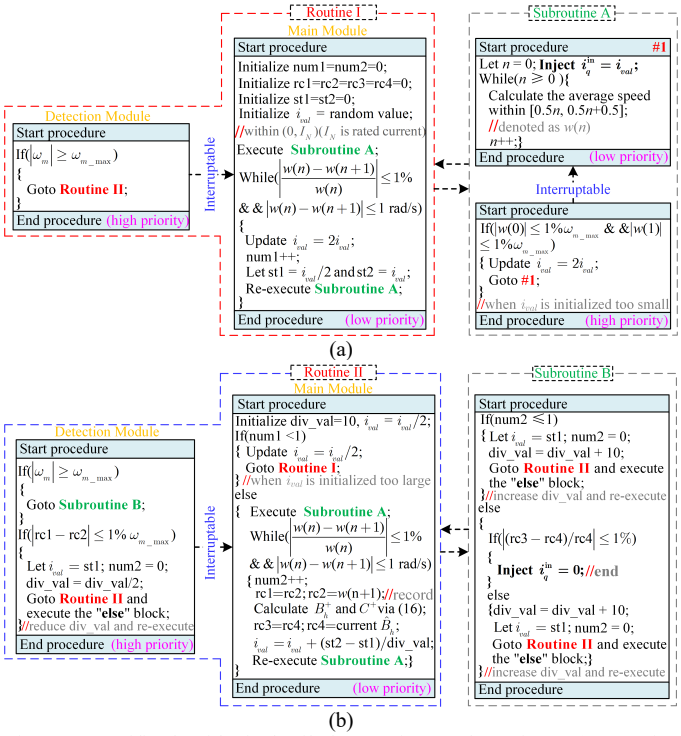

Fig. 20. Specific algorithmic details for Routine I and Routine II. (a) Routine I. (b) Routine II.

References

[1] C. Yang, B. Song, J. Jatskevich, H. Zhang, and C. H. T. Lee, "Normal-operation-undisturbed magnet flux linkage monitoring in PMSM drives via a mechanical-model-based dual time-scale approach," *IEEE Trans. Ind. Informat.*, vol. 20, no. 4, pp. 6266-6279, Apr. 2024.

[2] M. Xie, J. She, Z. Liu, and D. Li, "Online estimation of moment of inertia incorporating disturbance estimation," *IEEE Trans. Ind. Electron.*, vol. 71, no. 7, pp. 7610-7620, Jul. 2024.

[3] Y. Zuo, J. Mei, X. Zhang, and C. H. T. Lee, "Simultaneous identification of multiple mechanical parameters in a servo drive system using only one speed," *IEEE Trans. Power Electron.*, vol. 36, no. 1, pp. 716-726, Jan. 2021.

[4] C. Yang, B. Song, Y. Xie, and X. Tang, "Online parallel estimation of mechanical parameters for PMSM drives via a network of interconnected extended sliding-mode observers," *IEEE Trans. Power Electron.*, vol. 36, no. 10, pp. 11818-11834, Oct. 2021.

[5] D. Xiang, J. Yang, Y. Hao, and G. Xu, "Parallel-cascaded parameter identification scheme for PMSM-driven servo systems during self-commission," *IEEE Trans. Ind. Electron.*, early access, doi: 10.1109/TIE.2024.3417983.

[6] S. Yang and K. Lin, "Automatic control loop tuning for permanent-magnet AC servo motor drives," *IEEE Trans. Ind. Electron.*, vol. 63, no. 3, pp. 1499-1506, Mar. 2016.

[7] Y. Chen, M. Yang, J. Long, W. Qu, D. Xu, and F. Blaabjerg, "A moderate online servo controller parameter self-tuning method via variable-period inertia identification," *IEEE Trans. Power Electron.*, vol. 34, no. 12, pp. 12165-12180, Dec. 2019.

[8] K. Liu and Z. Zhu, "Fast determination of moment of inertia of permanent magnet synchronous machine drives for design of speed loop regulator," *IEEE Trans. Control Syst. Technol.*, vol. 25, no. 5, pp. 1816-1824, Sep. 2017.

[9] Q. Ni *et al.*, "A new position and speed estimation scheme for position control of PMSM drives using low-resolution position sensors," *IEEE Trans. Ind. Appl.*, vol. 55, no. 4, pp. 3747-3758, July-Aug. 2019.

[10] C. Yang, B. Song, Y. Xie, S. Zheng, and X. Tang, "Adaptive identification of nonlinear friction and load torque for PMSM drives via a parallel-observer-based network with model compensation," *IEEE Trans. Power Electron.*, vol. 38, no. 5, pp. 5875-5897, May 2023.

[11] L. Márton and F. van der Linden, "Temperature dependent friction estimation: Application to lubricant health monitoring," *Mechatronics*, vol. 22, no. 8, pp. 1078-1084, Dec. 2012.

[12] X. Zhang and Z. Li, "Sliding-mode observer-based mechanical parameter estimation for permanent magnet synchronous motor," *IEEE Trans. Power Electron.*, vol. 31, no. 8, pp. 5732-5745, Aug. 2016.

[13] S. Kobayashi, I. Awaya, H. Kuromaru, and K. Oshitani, "Dynamic model based auto-tuning digital servo driver," *IEEE Trans. Ind. Electron.*, vol. 42, no. 5, pp. 462-466, Oct. 1995.

[14] C. Lian, F. Xiao, S. Gao, and J. Liu, "Load torque and moment of inertia identification for permanent magnet synchronous motor drives based on sliding mode observer," *IEEE Trans. Power Electron.*, vol. 34, no. 6, pp. 5675-5683, Jun. 2019.

[15] F. Schutte, S. Beineke, A. Rolfsmeier, and H. Grotstollen, "Online identification of mechanical parameters using extended Kalman filters," in *Proc. IAS Annu. Meeting*, New Orleans, LA, USA, Oct. 1997, pp. 501-508.

[16] S. Beineke, F. Schütte, and H. Grotstollen, "Comparison of methods for state estimation and on-line identification in speed and position control loops," in *Proc. Eur. Conf. Power Electron. Appl.*, Trondheim, Norway, 1997, pp. 364-369.

[17] R. Garrido and A. Concha, "Inertia and friction estimation of a velocity-controlled servo using position measurements," *IEEE Trans. Ind. Electron.*, vol. 61, no. 9, pp. 4759-4770, Sept. 2014.

[18] C. Ilas, G. Griva, and F. Profumo, "On-line identification of mechanical parameters and load torque in induction machine field oriented drives," in

Proc. IEEE Int. Symp. Ind. Electron., Warsaw, Poland, Jun. 1996, pp. 985-989.
[19] M. Calvini, M. Carpita, A. Formentini, and M. Marchesoni, "PSO-based self-commissioning of electrical motor drives," *IEEE Trans. Ind. Electron.*, vol. 62, no. 2, pp. 768-776, Feb. 2015.
[20] Z. Liu, H. Wei, X. Li, K. Liu, and Q. Zhong, "Global identification of electrical and mechanical parameters in PMSM drive based on dynamic self-learning PSO," *IEEE Trans. Power Electron.*, vol. 33, no. 12, pp. 10858-10871, Dec. 2018.
[21] S. Kim, "Moment of inertia and friction torque coefficient identification in a servo drive system," *IEEE Trans. Ind. Electron.*, vol. 66, no. 1, pp. 60-70, Jan. 2019.
[22] C. Yang, B. Song, Y. Xie, S. Lu, and X. Tang, "Speed-controller-independent mechanical parameter identification in SPMSM drive achieved via signal injection," *IEEE Trans. Ind. Electron.*, vol. 70, no. 2, pp. 1282-1297, Feb. 2023.
[23] M. Fliess and H. Sira-Ramírez, "An algebraic framework for linear identification," *ESAIM: Control, Optim. Calculus Variation*, vol. 9, pp. 151-168, 2003.
[24] W.-S. Huang, C.-W. Liu, P.-L. Hsu, and S.-S. Yeh, "Precision control and compensation of servomotors and machine tools via the disturbance observer," *IEEE Trans. Ind. Electron.*, vol. 57, no. 1, pp. 420-429, Jan. 2010.
[25] C. Wang, J. Peng, and J. Pan, "A novel friction compensation method based on Stribeck model with fuzzy filter for PMSM servo systems," *IEEE Trans. Ind. Electron.*, vol. 70, no. 12, pp. 12124-12133, Dec. 2023.
[26] Y. Xie, X. Huang, and Z. Zhou, "Adaptive feed-forward friction compensation through developing an asymmetrical dynamic friction model," *Mech. Mach. Theory*, vol. 170, p. 104691, Dec. 2022.
[27] S.-H. Lee, J.-S. Yim, J.-H. Lee, and S.-K. Sul, "Design of speed control loop of a variable speed diesel engine generator by electric governor," in *Proc. IEEE Ind. Appl. Soc. Annu. Meeting*, 2008, pp. 1-5.

Chengbo Yang (IEEE Member) received the B.Eng. degree in mechanical design manufacturing and automation from Southwest University, Chongqing, China, in 2018 and the Ph.D. degree in mechanical engineering from Huazhong University of Science and Technology, Wuhan, China, in 2024.

He is currently a Postdoctoral Fellow at the Research Centre for Electric Vehicles and Department of Electrical and Electronic Engineering, The Hong Kong Polytechnic University, Hong Kong, China. He is also an active reviewer of IEEE Transactions on Industrial Electronics, IEEE Transactions on Power Electronics, and IEEE Transactions on Transportation Electrification. His research interests include motor drives, parameter estimation, motion control, control applications, and intelligent technology.

Wei Liu (IEEE Senior Member) received the B.Eng. and M.Eng. degrees in electrical engineering from China University of Petroleum, Qingdao, China, and the Ph.D. degree in electrical and electronic engineering from The University of Hong Kong (HKU), Hong Kong, China, in 2014, 2017, and 2021, respectively.

He is currently an Assistant Professor at the Research Centre for Electric Vehicles and Department of Electrical and Electronic Engineering, The Hong Kong Polytechnic University, Hong Kong, China. He is also an Honorary Assistant Professor at the Department of Electrical and Electronic Engineering, HKU, since 2023. Dr. Liu served as a Postdoctoral Fellow and then was promoted to a Research Assistant Professor from 2021 to 2023. He also worked as a Visiting Researcher with Nanyang Technological University, Singapore, in 2019. His research interests include electric vehicle technologies, wireless power transfer, power electronics, bioelectronics, and semiconductor devices.

Dr. Liu was the recipient of the Power Engineering Prize from HKU, two Gold Medals with Congratulations of the Jury in the International Exhibition of Inventions Geneva, the Excellent Paper Award, and the Best Presentation Award from international conferences in the area of Electric Vehicles and Transportation Electrification. He is also a Guest Associate Editor of IEEE Journal of Emerging and Selected Topics in Power Electronics, Associate Editor of international journals, and Session Chair of international conferences.

Songyan Niu received the B.Eng. degree in electrical engineering and automation from Central South University, Hunan, China, in 2017, and the M.Eng. degree in electronics and communication engineering from Harbin Institute of Technology, Harbin, China, in 2019, and the Ph.D. degree in electrical engineering from The Hong Kong Polytechnic University, Hong Kong, China, in 2024.

He is currently a Postdoctoral Fellow at The Hong Kong Polytechnic University, Hong Kong, China. His research interests include wireless power transfer technology and power electronics.

Jiahua Lyu received the B.Eng. degree in electrical engineering from Huazhong University of Science and Technology, Wuhan, China, in 2018, the M.S. degree in electronic engineering from The Hong Kong University of Science and Technology, Hong Kong, China, in 2019, and the Ph.D. degree in electrical engineering from The Hong Kong Polytechnic University, Hong Kong, China, in 2023.

He is currently a Postdoctoral Fellow at The Hong Kong Polytechnic University, Hong Kong, China. His research interests include computational electromagnetics, power electronics, and wireless power transfer.

Kwok Tong Chau (IEEE Fellow) received the B.Sc. (Eng.), M.Phil., and Ph.D. degrees in electrical and electronic engineering from The University of Hong Kong, Hong Kong, in 1988, 1991, and 1993, respectively.

He is currently a Chair Professor of electrical energy engineering with the Research Centre for Electric Vehicles and Department of Electrical and Electronic Engineering, The Hong Kong Polytechnic University, Hong Kong. He is the author of nine books and more than 350 journal papers. His research interests include electric and hybrid vehicles, power electronics and drives, and renewable energies.

Dr. Chau is a Fellow of the Institution of Engineering and Technology (IET), U.K., and of the Hong Kong Institution of Engineers. He is also a Co-editor for Journal of Asian Electric Vehicles. He is a Chartered Engineer. He was the recipient of the Changjiang Chair Professorship from the Ministry of Education, China, and the Environmental Excellence in Transportation Award for Education, Training, and Public Awareness from the Society of Automotive Engineers International.